# Comparisons of 2D IR measured spectral diffusion in rotating frames using pulse shaping and in the stationary frame using the standard method

S. K. Karthick Kumar,[a] A. Tamimi,[a] and M. D. Fayer[b]
*Department of Chemistry, Stanford University, Stanford, California 94305, USA*

(Received 7 September 2012; accepted 15 October 2012; published online 8 November 2012)

Multidimensional visible spectroscopy using pulse shaping to produce pulses with stable controllable phases and delays has emerged as an elegant tool to acquire electronic spectra faster and with greatly reduced instrumental and data processing errors. Recent migration of this approach using acousto-optic modulator (AOM) pulse shaping to the mid-infrared region has proved useful for acquiring two dimensional infrared (2D IR) vibrational echo spectra. The measurement of spectral diffusion in 2D IR experiments hinges on obtaining accurate 2D line shapes. To date, pulse shaping 2D IR has not been used to study the time-dependent spectral diffusion of a vibrational chromophore. Here we compare the spectral diffusion data obtained from a standard non-collinear 2D IR spectrometer using delay lines to the data obtained from an AOM pulse shaper based 2D IR spectrometer. The pulse shaping experiments are performed in stationary, partially rotating, and fully rotating reference frames and are the first in the infrared to produce 2D spectra collected in a fully rotating frame using a phase controlled pulse sequence. Rotating frame experiments provide a dramatic reduction in the number of time points that must be measured to obtain a 2D IR spectrum, with the fully rotating frame giving the greatest reduction. Experiments were conducted on the transition metal carbonyl complex tricarbonylchloro(1,10-phenanthroline)rhenium(I) in chloroform. The time dependent data obtained from the different techniques and with different reference frames are shown to be in agreement.  [http://dx.doi.org/10.1063/1.4764470]

## I. INTRODUCTION

Ultrafast two dimensional infrared (2D IR) spectroscopy has emerged as a powerful tool for experimentally examining fast molecular processes under thermal equilibrium conditions. This technique has been used for studying a variety of chemical and biological systems.[1–5] 2D IR can obtain a great deal of information about molecular systems. It provides both intramolecular structural insight by revealing vibrational couplings as well as intermolecular interactions through detailed 2D line shape analysis that can provide information on a vibrational chromophore's environment and its time evolution. In a number of important applications, such as protein structure,[6] long time scale aggregation of biomolecules,[7] or ground state thermal equilibrium chemical dynamics measured with vibrational echo chemical exchange spectroscopy,[4] the position of bands in a 2D spectrum or the change in amplitude of bands provides the important information. Detailed line shape analysis of the 2D IR bands is not necessary. However, in another important application spectral diffusion is measured. Spectral diffusion is the time evolution of the frequency of a vibrational mode of a molecule. The different frequencies of an ensemble of the molecules give rise to the inhomogeneously broadened linear IR absorption spectrum of the mode. For a molecule in a solvent or a vibrational probe in a protein, structural evolution of the system causes the vibrational frequency to evolve in time, i.e., undergo spectral diffusion. On a sufficiently long time scale, all structures that give rise to the inhomogeneously broadened absorption spectrum will be sampled, and spectral diffusion is complete. Spectral diffusion is observed by measuring the time dependence of the 2D line shape, rather than peak positions or amplitudes. As in linear absorption spectroscopy, it is more difficult to accurately measure a line shape than a line position or amplitude. The evolution of the inhomogeneously broadened 2D IR line shape becomes the main reporter on the surrounding structural dynamics. Such an analysis,[8,9] however, requires accurate line shape information. Avoiding or correcting line shape distortions is not usually a trivial consideration in most implementations of 2D-IR.

Several ways of implementing the 2D IR vibrational echo experiment have been discussed previously.[10,11] The experiments are third order non-linear spectroscopy. Three radiation field interactions with the sample give rise to a fourth field, which is the vibrational echo, the signal in the experiment. The most common implementation, which we will refer to as the standard implementation, involves crossing three non-collinear IR pulses in what is known as a box-CARS geometry, and then the vibrational echo is emitted in a unique direction. The pulses are time ordered by variable delay lines and spatially overlapped in the sample. The time between the first two pulses (interactions) will be referred to as $\tau$ and the time between the second and third pulses as $T_w$. The vibrational echo pulse is emitted at or after the third pulse. The time parameter for the vibrational echo emission is termed $t$ where the third interaction marks $t = 0$. To amplify the weak vibrational echo signal and to obtain phase information, a

[a]S. K. Karthick Kumar and A. Tamimi contributed equally to this work.
[b]Electronic mail: fayer@stanford.edu.

 

fourth pulse that does not pass through the sample, the local oscillator (LO), is overlapped with the signal for heterodyne detection. The combined echo and LO packet is sent into a monochromator used as a spectrograph, which effectively performs a "hardware" Fourier transform, which gives the vertical axis ($\omega_m$ axis) of the 2D spectrum. The data collection for a 2D spectrum for a given $T_w$ proceeds by scanning $\tau$. Scanning $\tau$ produces a temporal interferogram for each frequency, $\omega_m$. Numerically Fourier transforming the interferograms gives the horizontal axis ($\omega_\tau$) of the 2D spectrum. To produce an essentially purely absorptive spectrum (dispersive contribution minimized), two sets of signals are collected, the rephasing and non-rephasing signals. These can be collected by inverting the time ordering of the first two pulses, which corresponds to a sign change in $\tau$. With both pulses 1 and 2 at $\tau = 0$, first pulse 1 is scanned to negative time (less delay), and the interferogram is recorded. Pulse 1 is returned to $\tau = 0$, and pulse 2 is scanned to negative time, and the resulting interferogram is recorded. These two pieces are combined to give a complete interferogram.[12,13] Distortions in the 2D spectrum due to small inaccuracies in the time delays can be basically eliminated using active or passive phase stabilization techniques[14–16] and/or numerical corrections while processing the data. The latter process is known as "phasing" and involves correcting for errors in the absolute timing of $\tau$ and $t$.[12,13,17,18] The method briefly outlined ensures a line shape of sufficient quality that it has become the benchmark in studies involving line shape analysis.

One way to eliminate two uncertainties from the standard implementation is to change the phase matching such that the phasing and non-rephasing signals are emitted with the same wave vector. Since the emission wave vectors only differ in the sign of the term $\pm(\vec{k}_1 - \vec{k}_2)$, this can be done by setting $\vec{k}_1 = \vec{k}_2$, that is making the first two pulses collinear. Having the rephasing and non-rephasing signals emitted in the same direction ensures that they have the correct phase relationship since their sum is directly acquired. Having pulses 1 and 2 collinear also results in the echo being emitted collinearly with the third pulse, which then functions as the local oscillator for heterodyne detection. An important feature of having pulse 3 also act as the LO is that the echo field is phase-locked to the local oscillator field. The result is the elimination of experimental ambiguities except for the absolute $\tau$ timing. This geometry, for obvious reasons, is sometimes referred to as a pump-probe geometry, where the pump refers to the first two pulses and probe to the third. There are several drawbacks to this geometry. Pulses 1 and 2 each produces pump-probe signals with pulse 3 that are collinear with the echo signal. These pump-probe signals must be separated from the echo signal.[10,19] Another drawback that is present when collecting XXXX and XXYY polarization pathways is the inability to attenuate the LO without attenuating the signal since the signal is linear in the third pulse.[10] In the standard method, the LO is a separate pulse that can be attenuated so that is greater than but comparable to the echo $E$-field. The heterodyne detected signal is the so-called cross term $2\Re[L^*S]$, where $L$ is the LO electric field and $S$ is the echo signal electric field. This signal needs to be measured against $|L|^2$. Therefore, by reducing $L$, which does not change $S$, the cross-term $2\Re[L^*S]$ becomes a larger fraction of $|L|^2$. This is only possible in the collinear geometry when collecting the XYXY or YXXY pathways. The latter has been demonstrated in the visible[20] as well as in the mid-IR.[21,22]

The importance of the collinear geometry is that it permits the use of Fourier-domain pulse shaping,[23] a technique pioneered by Warren in the visible regime.[24–26] Fourier-domain pulse shaping in the mid-infrared region and its use for 2D IR spectroscopy in a pump-probe geometry was pioneered by Zanni and co-workers.[10,27,28] In addition to the elimination of experimental issues associated with phase problems that can distort a 2D spectrum, the pulse shaping collinear method has many other advantages. It greatly reduces the time spent moving precision mechanical delay lines and eliminates the laser shots lost in "chopping" one of the optical beams which is necessary to subtract out the $|L|^2$ term to recover $2LS$. In addition, the pulse shaping collinear method allows the user to have complete control over the phase of the individual pump pulses (pulses 1 and 2), which is important for implementing various phase-cycling schemes for scatter removal, chopping and data acquisition in a rotating frame.[10,29] A singularly attractive feature of pulse-shaping based 2D IR is the faster data acquisition made possible when the data are collected in a rotating frame of reference.

The pulse shaping method has been applied in a number of 2D IR applications.[7,30] However, none of these have involved the determination of accurate 2D line shapes and their time evolution, which are necessary to measure spectral diffusion. It is important to determine if the pulse shaping method can produce accurate line shape and spectral diffusion data. Here we present data measuring spectral diffusion on a single molecular system using the standard 2D IR method and the pulse shaping collinear method. The standard method yields data in the stationary frame. With the pulse shaping system we obtain data in the stationary frame, a partially rotating frame (detuned from the transition frequency by $\sim$37 cm$^{-1}$), and for the first time in the fully rotating frame. The data from the pulse shaper based 2D IR setup in a stationary frame were collected using a phase cycling scheme by Zanni and coworkers and the data in partially and fully rotating frame were collected using a novel phase cycling scheme put forward by Yan and Tan.[19] We show that the collected data from all the phase cycling schemes and the data from standard 2D IR setup are in essentially perfect agreement. However, the length of time necessary to collect data with the pulse shaping system is substantially reduced in all experiments, with a vast reduction using the fully rotating frame and the slightly detuned partially rotating frame.

## II. EXPERIMENTAL PROCEDURES

### A. Optical setup

The interferometry part of the experimental setup is shown in Figure 1(a). The mid-IR source is an optical parametric amplifier[31] pumped by a regeneratively amplified Ti:Sapphire femtosecond laser source. The system used for these experiments consists of a 1 kHz regenerative amplifier pumped by 527 nm, 1 kHz, Nd:YLF laser (Darwin Pro,

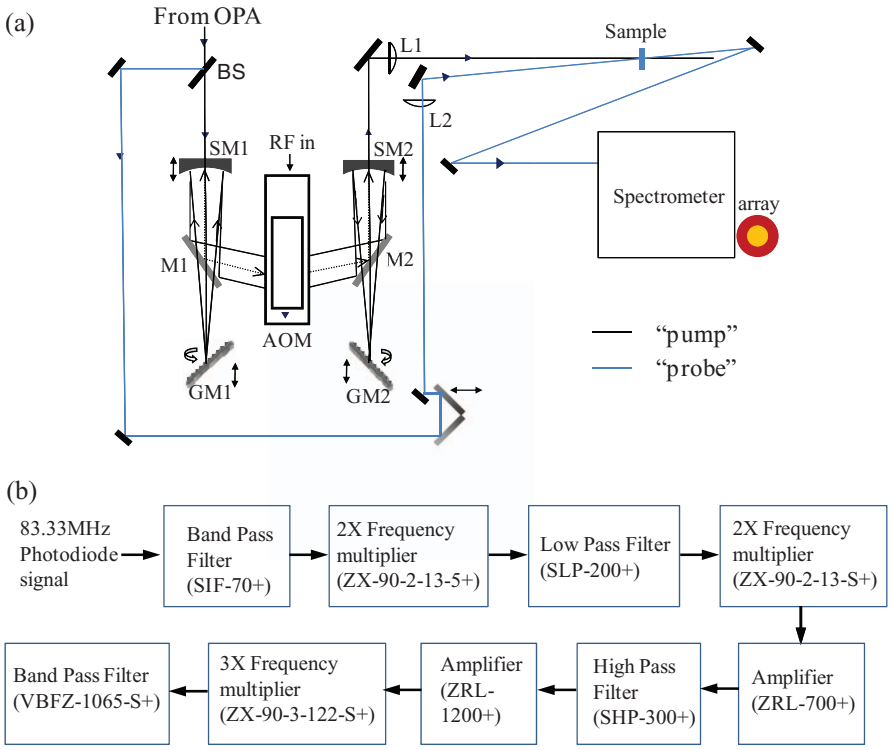


FIG. 1. (a) Schematic of the 2D-IR pulse-shaping setup. OPA: optical parametric amplifier, BS: beam splitter, SM: spherical mirror, M: mirror, GM: grating, AOM: acousto-optical modulator, RF: radio-frequency wave, L: lens. (b) Schematic of the 12× frequency multiplier circuit used to generate the clock signal for the AWG at a frequency close to 1 GHz. The part numbers from Mini-Circuits® are shown in parentheses.

Model 527-30-M, Quantronix) and seeded by 80 fs pulses from a Ti:Sapphire oscillator (Model TIF-50, Atseva LLC) with a repetition rate of 83.33 MHz and wavelength centered at 800 nm. The oscillator is pumped by a 532 nm Nd:$YVO_4$ CW laser (Sprout S-G-5W, Lighthouse Photonics). The repetition rate of the Ti:Sapphire oscillator was customized to be 83.33 MHz so that a photodiode signal can be converted to 1 GHz using a 12× multiplier circuit as discussed later. 100 fs pulses with 650 $\mu$J of energy centered at 800 nm from the regenerative amplifier were used to pump a homebuilt mid-IR optical parametric amplifier to generate ~170 fs pulses (~90 $cm^{-1}$ FWHM bandwidth) centered at 2027 $cm^{-1}$ with ~5 $\mu$J of pulse energy. The mid-infrared pulses were then co-aligned with a He-Ne beam and a 90:10 ZnSe beam splitter was used to split the incoming pulse to a weaker probe pulse and a stronger pump pulse. The weak pulse is routed through a mechanical delay line which is used to set $T_w$.

The strong pulse was sent to a mid-infrared Fourier-domain pulse-shaper. The pulse-shaper consists of a wide-aperture germanium acousto-optic modulator (AOM) (Model LS600-1109-10W, 3–12 $\mu$m AR coated, ISOMET) placed at the Fourier plane of a 4-*f* pulse-shaping geometry as described by Zanni and coworkers[10,27,28] with some modifications. By using 240 line gratings (Newport, Model 53067BK02-820R), and 200 mm focal length curved mirrors, we obtain good resolution for our spectral bandwidth. The resolution is ~3 nm FWHM per "pixel." This is determined during the calibration procedure. In this procedure, spikes with well-defined timing, created by setting specific time points in the RF buffer to have a high voltage level, are sent to the AOM. These spikes diffract specific frequencies which are resolved by the spectrometer and plotted against the corresponding timing of the spikes. This procedure provides the mapping between the time axis of the RF waveform and the frequency axis of the spatial Fourier plane of the pulse shaper.[7] The width of the spikes in the frequency domain is the resolution of the shaper and compares well with numbers obtained from other diagnostics of the shaping resolution. The aperture passes ~900 nm at the experimental wavelength, which yields approximately ~300 effective pixels, ~250 of which are usually used. Another modification is that the curved mirrors are spherical rather than cylindrical. The mirrors were cut 5 mm above the center to allow the input and output beams to pass above them while minimizing the vertical folding angle. At our current power and resolution, nonlinear effects in the germanium are negligible when the pulse is frequency-resolved. When the pulse is not frequency-resolved, significant absorption is seen even with cylindrical optics. We found the diffraction efficiency to be comparable (around 50% total shaper throughput), but the spherical optics permit easier alignment. This is important since errors in focusing using cylindrical optics can be compensated for by spatial chirp which makes it difficult to detect beam ellipticity using traditional beam characterization techniques which are quite tedious.

Gaussian beam propagation analysis of the pulse shaper with a 20 mm thick Germanium crystal at the Fourier plane indicates that for a properly collimated beam at the output of the pulse shaper, the focus of the 200 mm curved mirror should be ~2.5 mm into the first surface of the germanium slab in the AOM. This focusing places the vertical beam waist and

the Fourier plane in the center of the germanium slab which yields symmetric alignment on the two sides of the AOM. Detailed descriptions and methods of alignment, calibration, and optimization of the output pulses for similar devices can be found elsewhere.[7,23] The output beam from the pulse shaper is focused into the sample using a 150 mm focal length $CaF_2$ lens and the weak probe pulse is focused in the sample using a 100 mm focal length $CaF_2$ lens. The probe is collimated after the sample then dispersed in a spectrometer which images the spectrum onto a 32 element HgCdTe infrared array detector.

### B. Electronics and timing

A 1 GS/s arbitrary waveform generator (AWG) (Model CG11G2, GaGe-Applied) with 16 Megasamples of on-board memory was programmed to generate the necessary waveforms. The RF waveforms were then amplified by an RF power amplifier (Model RFA1160/4, ISOMET) and sent to the AOM which has piezoelectric transducers that convert the RF waveforms to acoustic waveforms traveling along the germanium AOM crystal which has an active aperture of 10 mm $\times$ 55 mm. The acoustic waveforms travel along the germanium at a speed of 5.5 mm/$\mu$s. This requires the duration of RF waveforms to be 10 $\mu$s to fill the entire AOM aperture. The AWG requires an external clock signal at 1 GHz for better phase stability.[28] Since our femtosecond oscillator was customized to run at 83.33 MHz repetition rate, a frequency very close to 1 GHz was derived from the photodiode signal of the femtosecond oscillator using a 12$\times$ multiplier circuit. A sequence of components from Mini-Circuits with model numbers used for 12$\times$ frequency multiplication is shown in Figure 1(b). The AWG card can also be externally clocked from $\sim$973 MHz to $\sim$1005 MHz which allows signals derived from other oscillator repetition rates to be used. Part of the photodiode signal from the oscillator was also used to clock an 8 channel digital delay generator (Quantum Composers 9538) which generates the gate signal for the RF amplifier as well as triggers signals at appropriate delays for the regenerative amplifier pump laser and Pockels cells, the AWG card, and the MCT array electronics. Accuracy and stability of the triggers are essential. The RF signal that goes into the AOM must start more than 20 $\mu$s before the arrival of the IR pulse at the AOM. Time jitter results in jitter in the outgoing IR shaped pulses. Synchronization of better than 100 ps is achieved, which is necessary for stable shaped pulses.

### C. Phase cycling schemes and reference frames

One of the great advantages of pulse shaping is the control it provides over the phase of the pulses. This is useful in multidimensional spectroscopy because it allows one to select out the desired signal or a set of signals through their dependence on the phase of the pump pulses, a technique known as phase-cycling.[26,29,32] Phase-cycling not only provides the technique with flexibility that is absent in techniques which rely purely on wave vector phase matching but also speeds acquisition by eliminating the need for mechanical chopping of one or more of the input beams. With phasing cycling the utility of chopping is achieved but data are acquired on every laser shot.[10,19]

A phase-cycle consists of repeating the acquisition sequence in an experiment multiple times, each time with the laser pulses having a particular set of phases. The resulting signals are then multiplied by a corresponding set of coefficients and summed. There are multiple possible phase cycles that can be used in a 2D IR experiment. Which one is used depends on the how selective the experiment needs to be in terms of which unwanted signals must be rejected. The less selective, the more economical the phase cycle can be in terms of the number of shots. A general theory which describes in detail how to arrive at the most economical phase-cycle for a given application was worked out by Yan and Tan.[19] We will briefly outline it here. For the pump-probe geometry described above, the first two interactions occur with one or two pulses in the pump direction, and the third interaction defines the probe direction. All signals along the probe direction are collected and therefore heterodyne with the third pulse.

The phase dependence of these collected signals can be represented as

$$S_\beta(\tau, T_w, \omega_m) = F_\beta(\tau, T_w, \omega_m)e^{i\beta\phi_{1,2}}, \tag{1}$$

where $\beta$ is an integer which depends on the type of signal, and is 1 for the echo signals and 0 for the pump-probe signals, $\omega_m$ is the monochromator detection frequency and $\phi_{1,2}$ is the relative phase between the first two pulses. The signal corresponding to a particular $\beta$ can be extracted by a discrete Fourier transform along $\phi_{1,2}$. By repeating the acquisition for different $\phi_{1,2}$ values while keeping the other parameters the same, the phase interval $[0, 2\pi]$ can be discretely sampled and weighed in the following manner:

$$S_\beta = \frac{1}{L}\sum_{l=0}^{L-1} \tilde{S}(\phi_{1,2} = l\Delta\phi)e^{-il\beta\Delta\phi}, \tag{2}$$

where the dependence on other parameters has been suppressed, $\tilde{S}$ is the acquired signal, and $\Delta\phi = \frac{2\pi}{L}$. Mathematically, this procedure cannot distinguish between signals having $\beta = \beta_0$ and signals having $\beta = \beta_0 + nL$ where $n$ is an integer. The choice of $L$ therefore depends on what contamination from other signals is acceptable. For $L = 1$, the background and pump-probe signals ($\beta = 0$), as well as positive and negative frequency copies of the echo signal ($\beta = \pm 1$) are acquired. The background and pump-probe signals are eliminated using $L = 2$, whereas $L = 3$ isolates the positive frequency echo uniquely ($\beta = 1$). This will become important in the context of acquisition in the rotating frame. Important is also the ability to eliminate scatter by subtracting shots where the absolute phase of the two pump pulses is inverted or shifting it away from the relevant data through phase incrementation.[10]

Let $S_E$ be the echo signal ($\beta = 1$), we can then express the acquired signal in the following form:

$$S_E(\tau, T_w, \omega_m) = F(\tau, T_w, \omega_m)e^{i\omega_0\tau}e^{i\phi_{1,2}}, \tag{3}$$

where $\omega_0$ represents the center of the line and $F$ contains the line shape information, which for an inhomogeneously broadened absorption line includes small frequency shifts of

the order of the line shape. Suppose that during the $\tau$ scan, $\phi_{1,2}$ is replaced by $\phi_{1,2} - \omega_f\tau$ where $\omega_f$ is a conveniently chosen frame rotation frequency. The acquired signal now becomes

$$S_E(\tau, T_w, \omega_m) = F(\tau, T_w, \omega_m)e^{i(\omega_0-\omega_f)\tau}e^{i\phi_{1,2}}, \quad (4)$$

which oscillates at $\omega_0 - \omega_f$. For $\omega_f = 0$, the signal oscillates rapidly at the vibrational resonance frequency, which imposes a high time sampling rate for line shape reconstruction by the Nyquist–Shannon sampling theorem.[33] We term this acquisition in the stationary frame. The stationary frame is used in standard 2D IR where there is no practical technique for implementing a rotating frame. The other limiting case where $\omega_f = \omega_0$, the acquired signal does not oscillate with $\tau$ at any frequency larger than the linewidth. We refer to this case as acquisition in a fully rotating frame. In the case where there are multiple peaks of interest spanning a range in $\omega_\tau$ larger than the linewidth, the criterion becomes the difference between $\omega_f$ and the farthest desired frequency along the $\omega_\tau$ axis. An important consideration when taking data in a fully rotating frame is the overlap of positive and negative frequency signals ($\beta = \pm 1$)[19] which renders a two-point phase cycle unusable. For this reason, the rotating frame data were acquired using the three-point phase cycle referred to above ($L = 3$), which permits the extraction of the positive frequency signal without interference from the negative frequency signal.[19,29] While advantageous in relaxing sampling rate restrictions, there is higher noise at zero frequency.[10] Therefore, it is necessary to decide if the increased averaging in a unit time makes up for the increased noise. The fully rotating frame has not been used previously in the IR, although it has very recently been demonstrated in the visible.[34] The intermediate case of a partially rotating frame[10] has the line shifted from zero frequency, but the shift is still small enough to permit a relatively large sampling interval. The bandwidth of the time domain signal in this case can be roughly calculated as the difference between $\omega_f$ and the farther bound for the $\omega_\tau$ axis in the acquired frequency range.

### D. Sample preparation and the FT-IR absorption spectrum

Pentacarbonylchlororhenium(I) ($Re(CO)_5Cl$, STREM) and 1,10-phenanthroline (phen, Aldrich) were purchased from commercial sources and were used without further purification. Tricarbonylchloro(1,10-phenanthroline)rhenium(I) (*fac*-$Re(phen)(CO)_3Cl$, henceforth "rhenium complex") was synthesized according to a literature synthesis.[35]

A 500 $\mu$M solution of the rhenium complex in chloroform was prepared and the solution was sandwiched between two calcium fluoride windows separated by a 100 $\mu$m Teflon annular spacer. The FT-IR absorption spectrum of this sample was collected using a Thermo Scientific Nicolet 6700 FT-IR spectrometer. Figure 2 shows the normalized absorption spectrum corresponding to the three carbonyl stretching modes, $\nu_1$, $\nu_2$, and $\nu_3$ in order of increasing frequency. The $\nu_3$ or nearly symmetric CO stretch, which was studied in these experiments, had an absorbance of ~30 mOD at ~2027 $cm^{-1}$ with a FWHM of ~8 $cm^{-1}$. The $\nu_1$ and $\nu_2$ modes, which appear at ~1900 $cm^{-1}$ and ~1928 $cm^{-1}$ respectively, are partially unresolved. The bandwidth of the laser system is ~100 $cm^{-1}$ FWHM, so only the $\nu_3$ mode was pumped.

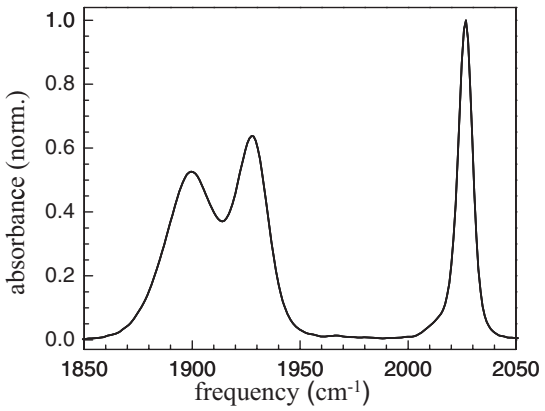


FIG. 2. Normalized linear FT-IR spectrum of the carbonyl stretching modes of the linear complex in chloroform. The modes are, left to right, $\nu_1$ = ~1900 $cm^{-1}$, $\nu_2$ = ~1928 $cm^{-1}$, and $\nu_3$ = ~2027 $cm^{-1}$.

### E. 2D IR vibrational echo experiments

Data were collected on the $\nu_3$ mode of the rhenium complex described above using the pulse-shaper based setup. Three sets of data were acquired with three different reference frame rotation frequencies. The stationary frame data were acquired with no frame rotation ($\omega_f = 0$). The partially rotating frame data were collected at $\omega_f$ = 1990 $cm^{-1}$, which is 37 $cm^{-1}$ detuned from the peak. Finally, the fully rotating frame data were acquired with $\omega_f$ = 2027 $cm^{-1}$. For all three sets of data, $T_w$ was scanned from 0.26 ps to 60 ps using a mechanical delay line. For the stationary frame data, $\tau$ was scanned from 0 to 7 ps in 4 fs steps. For the partially and fully rotating frame data, $\tau$ was scanned from 0 to 7 ps in 100 fs steps. The conventional 2D IR spectra covered a $T_w$ range from 0.5 ps to 11 ps and is the same data published previously in another context.[1] Details of the acquisition process are included in the supporting information for that paper.

## III. RESULTS AND DISCUSSION

### A. Comparison of the spectral diffusion measurements

Examples of the experimental interferograms are shown in Figure 3. For the stationary frame interferogram the sampling time step ($\tau$) of 4 fs is about double the Nyquist-Shannon requirement for this frequency, allowing adequate reconstruction. This time step requires 1750 time points, which is about as many buffers as the AWG memory of 16 megasamples can hold even without any phase-cycling. The phasing cycling is required to eliminate the two pump-probe signals that are associated with pulses 1 and 3 and pulses 2 and 3. With phase-cycling, the complete $\tau$ scan will not fit in the memory of the AWG even when sampling at the Nyquist-Shannon requirement. To obtain the full $\tau$ scan necessitated breaking it down into multiple shorter sections. Breaking the

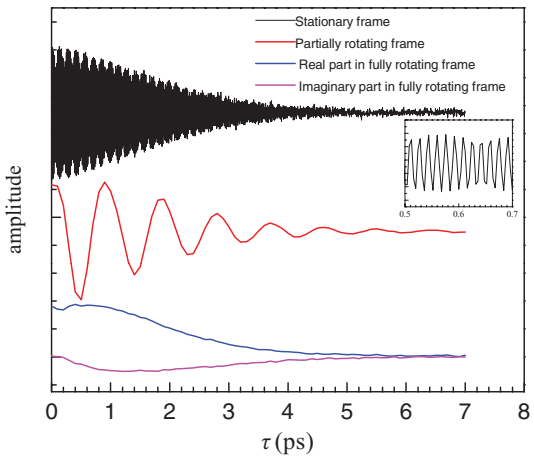


FIG. 3. Sample interferograms collected for the same sample in different reference frame. Top to bottom, these are in a stationary frame, a partially rotating frame ($\omega_f = 1990\ \text{cm}^{-1}$), and a fully rotating frame ($\omega_f = 2027\ \text{cm}^{-1}$). The traces have been offset for clarity. The inset shows a section of the stationary frame interferogram between 0.5 and 0.7 ps. The apparent amplitude modulation is due to the discreet time sampling.

$\tau$ scan into several sections requires additional experimental time for reconfiguring the AWG for each section of the scan. For the partially and fully rotating frames, the sampling time step of 100 fs is more than eight times the Nyquist-Shannon requirement. In the rotating frames it was only necessary to take 70 $\tau$ points. For the length of the $\tau$ scans in these experiments, the entire scan with phase cycling could be fit in the AWG memory.

The interferograms collected were Fourier-transformed along the $\tau$ dimension to yield the $\omega_\tau$ axis for each 2D spectrum taken at a given $T_w$. The $\omega_m$ axis is the spectrometer detection frequency. Examples of spectra taken with the standard method (stationary frame) using delay lines as well as using the pulse shaping method in the stationary, partially rotating, and fully rotating frames are shown in Figure 4. 2D spectra at two $T_w$s are shown for each method. The positive going bands (red) arise from the 0-1 vibrational transition. The negative going bands (blue) come from vibrational echo emission at the 1-2 vibrational frequency. Only part of the 1-2 bands are shown. The 1-2 bands are shifted to lower frequency along the $\omega_m$ axis by the vibrational anharmonicity. The spectra are essentially identical. There are very slight differences between the full rotating frame data and the partial rotating frame data, which we believe are due to systematic noise present at zero frequency. Shifting the frame rotation frequency does not shift these artifacts away from zero frequency. If there are in fact systematic noise artifacts at zero frequency, it may be advantages to select a frame rotation frequency which preserves the benefits of a fully rotating frame in relaxing sampling restrictions while avoiding such noise. However, as shown below, any zero frequency noise artifacts do not affect the ultimate goal of the experiments, which is to measure spectral diffusion by the $T_w$ dependence of the 2D line shape. There may also be minor differences between the data collected using the standard setup and the data collected using our pulse-shaping setup. These minor line shape distortions may result from the manual phasing and data post-

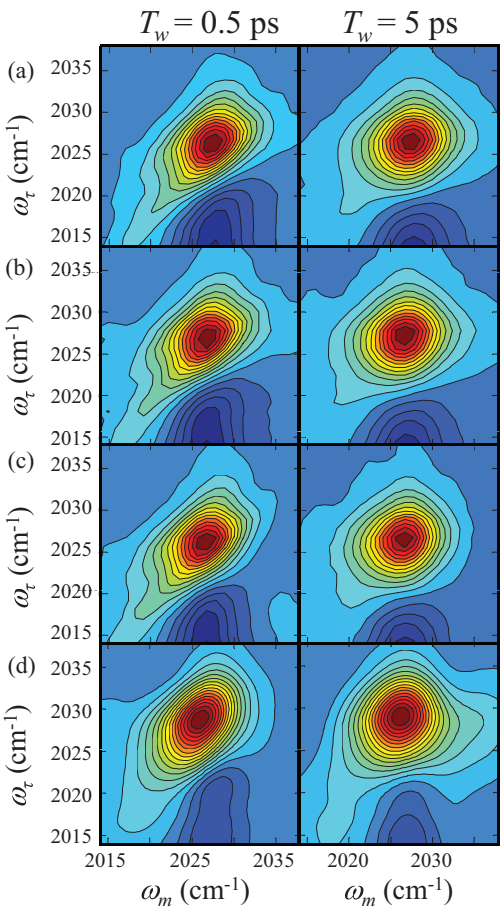


FIG. 4. Sample 2D spectra collected in multiple reference frames at two waiting times, $T_w = 0.5$ ps and $T_w = 5$ ps. The reference frames are in order (a) stationary frame, (b) partially rotating frame, (c) fully rotating frame, and (d) stationary frame using a standard setup.[1]

processing in standard 2D IR.[13] One of the advantages of the pulse-shaping method is that the vibrational echo signal is self-heterodyned by pulse 3 and the relative phase of pulses 1 and 2 is not subject to uncertainty. The resulting data therefore have the correct phases, and there is no need for post data collection corrections that are virtually unavoidable when using the standard 2D IR vibrational echo method. Again, any small differences do not affect the determination of the spectral diffusion.

As just alluded to, the important question is whether the different data acquisition methods affect relevant information derived from the $T_w$ dependent line shapes, which ultimately yield the frequency-frequency correlation function. To assess this, we analyzed all of the $T_w$ dependent 2D IR spectra using the center line slope (CLS) method[8,9] to extract the frequency-frequency correlation function (FFCF). The CLS$\omega_m$ method consists, briefly, in taking slices of the 2D spectra parallel to the $\omega_m$ axis for a range of $\omega_\tau$ surrounding the peak of the diagonal 0-1 transition. Each slice is a spectrum. Only the peak of each slice spectrum is necessary. The peak of each slice is obtained by fitting it to a Gaussian function around the peak amplitude. A plot of the peak positions ($\omega_m$, $\omega_\tau$) is plotted. These peak positions form a line, the center line. The slope of the line, the center line slope,

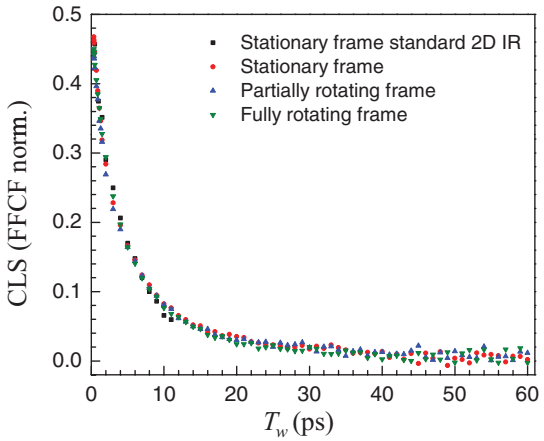


FIG. 5. The CLS plots resulting from analysis of the 2D spectra.

is determined. This procedure is repeated for every spectrum and the resulting CLS data are plotted against the corresponding $T_w$ of the individual spectra. The resulting CLS plot is the normalized FFCF.[8] The complete FFCF is obtained from the CLS data and the vibrational absorption spectrum.[8]

The CLS data for the four types of experiments are displayed in Figure 5. Clearly, the data are identical within the noise. The agreement between the standard method data and the pulse-shaping based data is important since the standard data serve as the benchmark. The close agreement over the whole 60 ps range of the three pulse-shaping based data sets, as well as the remarkable similarity of the spectra themselves, serves to demonstrate that the pulse-shaper is indeed controlling the spectral phase of the pulses accurately and without distortion. This frees the user to set the frame rotation frequency according to the considerations outlined in this paper or other considerations without additionally worrying about accuracy of the resulting line-shapes. This is the first demonstration that the pulse-shaping based method in the stationary and rotating frames can be used to determine accurate line-shapes, and therefore, the FFCF which provides information on a system's structural dynamics.

### B. The frequency-frequency correlation function

The main purpose of this paper is to demonstrate that accurate time dependent 2D IR line shapes, which are used to measure spectral diffusion, can be obtained using pulse shaping techniques in the rotating and stationary frames. Figure 5 shows that the CLS data are independent of the method used. Figure 5 almost certainly contains the most detailed measurements of spectral diffusion because of the number of points and the low level of point-to-point noise in the data. Therefore, it is worth briefly commenting on the results of the spectral diffusion measurements.

The CLS data in Figure 5 were fit to a tri-exponential decay. Statistical analysis showed that three exponentials are necessary to characterize the data. This fit was compared to a biexponential fit using the Akaike information criterion,[36] and the tri-exponential model was found to be many orders of magnitude more likely to be correct. The CLS fit yields three time constants and three associated amplitude factors.[8,9] The CLS is normalized, and the difference between the value of the CLS curve at $T_w = 0$ and 1 is related to the homogeneous component of the FFCF. By combining the CLS data and the absorption line shape, the homogenous component is determined.[8,9]

The FFCF is modeled as a sum of exponential factors representing the various timescales on which frequency-frequency decorrelation takes place[37]

$$C_1(t) = \langle \delta\omega_{1,0}(\tau_1)\delta\omega_{1,0}(0)\rangle = \sum_i \Delta_i^2 \exp(-t/\tau_i), \qquad (5)$$

where the $\Delta_i$ are the frequency fluctuation amplitudes of each component, and the $\tau_i$ are their associated time constants. A component of the FFCF where $\Delta\tau \ll 1$ is termed motionally narrowed, and is the dominant source of the homogeneous broadening of the absorption line. When a component is motionally narrowed, $\Delta$ and $\tau$ cannot be determined separately. The motionally narrowed homogeneous contribution to the absorption spectrum has a pure dephasing width given by $\Gamma^* = \Delta^2\tau = 1/\pi T_2^*$, where $T_2^*$ is the pure dephasing time, and $\Gamma^*$ is the pure dephasing linewidth. Though in condensed phase systems, the homogenous linewidth is dominated by pure dephasing, the observed homogenous dephasing time, $T_2$, also has contributions from the vibrational lifetime and orientational relaxation:

$$\frac{1}{T_2} = \frac{1}{T_2^*} + \frac{1}{2T_1} + \frac{1}{3T_{\text{or}}}, \qquad (6)$$

where $T_2^*$, $T_1$, and $T_{\text{or}}$ are the pure dephasing time, vibrational lifetime, and orientational relaxation times, respectively. The total homogeneous linewidth is then $\Gamma = 1/\pi T_2$. Here the combination of the lifetime and orientational relaxation contribute $\sim$1 cm$^{-1}$ to the total homogeneous linewidth.

The FFCF parameters are given in Table I. The $\Delta_i$ are the standard deviations of amplitude factors, which combine to give the inhomogeneous linewidth. The total inhomogeneous contribution to absorption linewidth is the convolution of the Gaussian standard deviations. The inhomogeneous FWHM is 5.9 cm$^{-1}$. The Lorentzian homogeneous component has a FWHM of 4.6 cm$^{-1}$. The total line is the convolution of the Gaussian and Lorentzian component, which is a Voigt line shape. The homogenous component (motionally narrowed) highlights the role of rapid solvent dynamics in dephasing. Processes such as very fast density fluctuations and ballistic collisions within the first solvent shell are expected to contribute.

TABLE I. FFCF parameters for the rhenium complex in chloroform.

| $T_2$ (ps) | $\Gamma$ (cm$^{-1}$) | $\Delta_1$ (cm$^{-1}$) | $\tau_1$ (ps) | $\Delta_2$ (cm$^{-1}$) | $\tau_2$ (ps) | $\Delta_3$ (cm$^{-1}$) | $\tau_3$ (ps) |
|---|---|---|---|---|---|---|---|
| 2.30 ± 0.02 | 4.62 ± 0.03 | 1.47 ± 0.05 | 1.1 ± 0.2 | 1.90 ± 0.06 | 5.4 ± 0.5 | 0.77 ± 0.3 | 25 ± 4 |

The $\tau$ values should be viewed as time scales rather than a well-defined time constant of a single process. Here we will present some ideas of processes that could contribute to the spectral diffusion on the various time scales in the FFCF. The fast inhomogeneous process ($\tau_1 = 1.1$ ps) may arise from fluctuations within the first solvent shell. The polarity of chloroform is expected to cause an inhomogeneous and fluctuating local electric field. The strength of the solvent interaction with the Re complex in chloroform is reinforced by the wider and more inhomogeneous line observed in chloroform compared to dichloromethane. The failure of the rhenium complex to significantly dissolve in carbon tetrachloride further suggests relatively strong solvation interactions in chloroform. Small density fluctuations from motions of the solvent around the complex can occur on the 1 ps time scale. In pure chloroform a molecule will diffuse ~1 Å in a ps.

The intermediate time scale process ($\tau_2 = 5.4$ ps) is suggestive of effects involving the reorientation of solvent molecules around the Re complex solute. Part of the inhomogeneous broadening can be caused by different distributions of chloroform orientations around different solute molecules. The experimentally determined orientational relaxation time constant in bulk chloroform is 3.3 ps, which was measured using optical heterodyned detected optical Kerr effect (OHD-OKE) experiments.[38,39] Here we are interested in solvent molecules in the first solvation shell of the solute. The presence of the solute may increase the orientational relaxation time. Furthermore, it is important to recognize that the orientational relaxation correlation function, the second Legendre polynomial correlation function, obtained from the OHD-OKE experiments is a different correlation function than the FFCF. Therefore, the resulting time constants cannot be directly compared. Nonetheless, the time scales are similar enough to be suggestive. Finally, the slowest time scale process ($\tau_3 = 25$ ps) may be caused by structural fluctuations involving longer length scales such as diffusion of solvent molecules resulting in variations in coordination number.[40,41]

In conducting these experiments, some of the advantages of the pulse-shaping approach became strikingly apparent. The speed with which the data were acquired was in sharp contrast to the conventional method. Over 70 spectra in the $T_w$ series were acquired in six to ten hours compared to the multiple days it takes with a standard setup. Although a direct comparison is not straightforward, a single $T_w$ point acquired using a standard 2D IR setup in our lab for this sample requires almost 3 hours. Superior signal to noise is achieved using the pulse shaping setup in under ten minutes. This speed is also accompanied by results which have proven to be lower in noise and more reproducible. Therefore, more data can be taken and with greater confidence. It is important to note, in this context, that an assertion that the CLS data require tri-exponential fitting could not have been made without having such low-noise CLS data which adequately sample the time domain dependence. Moreover, while most of the data acquired with the pulse-shaping setup are for vibrational modes with strong transition dipoles, such as metal carbonyls, recent tests have shown that very low absorbance samples (less than 1 mOD) and vibrations with weak transition dipoles (nitriles) also yield good data, but the acquisition time increases dramatically. Some of the metal carbonyl spectra acquired in our lab have complex spectra with multiple overtone bands and fifth order peaks. This complexity and the broader spectral range covered in the spectra have not proven any more challenging to acquire using the pulse shaping system.

It is worth noting that there are similar applications for pulse shaping in multidimensional visible spectroscopy.[42] While direct applicability is difficult to assert, this study is a proof of principle that accurate line shapes can be obtained.

## IV. CONCLUDING REMARKS

We have implemented a pulse-shaping based 2D IR vibrational echo experiment in a pump-probe geometry. Data were taken using this setup on a previously studied metal carbonyl complex, *fac*-Re(phen)$(CO)_3$Cl, in a stationary, a partially rotating, and a fully rotating acquisition frame. The spectra themselves, resulting from these data as well as the data previously acquired using a standard delay line setup, were found to be identical within the noise. Furthermore, the spectral diffusion information derived from them, in the form of a CLS analysis, was shown to be the same regardless of origin. The speed of data acquisition and the quality of the CLS derived from the pulse-shaping setup were both found to be superior to those derived from the standard setup. The results augment previous uses of the pulse-shaping method[7,30] by demonstrating that accurate line shapes and spectral diffusion can be measured in the stationary, partially rotating, and fully rotating frames.

## ACKNOWLEDGMENTS

This work was funded by the Division of Chemical Sciences, Geosciences, and Biosciences, Office of Basic Energy Sciences of the U.S. Department of Energy through Grant No. DE-FG03-84ER13251 and by the Air Force Office of Scientific Research Grant No. FA9550-12-1-0050. We would also like to thank Adam L. Sturlaugson, supported by the National Science Foundation Grant No. CHE-1157772 for performing the optical heterodyne detected optical Kerr effect measurements.

[1] D. E. Rosenfeld, Z. Gengeliczki, B. J. Smith, T. D. P. Stack, and M. D. Fayer, Science **334**, 634–639 (2011).
[2] M. D. Fayer, Ann. Rev. Phys. Chem. **52**, 315–356 (2001).
[3] M. D. Fayer, D. E. Moilanen, D. Wong, D. E. Rosenfeld, E. E. Fenn, and S. Park, Acc. Chem. Res. **42**, 1210–1219 (2009).
[4] M. D. Fayer, Annu. Rev. Phys. Chem. **60**, 21–38 (2009).
[5] Y. S. Kim and R. M. Hochstrasser, J. Phys. Chem. B **113**(24), 8231–8251 (2009).
[6] A. Remorino and R. M. Hochstrasser, "Three-dimensional structures by two-dimensional vibrational spectroscopy," Acc. Chem. Res. (to be published).
[7] C. Middleton, A. Woys, S. Mukherjee, and M. Zanni, Methods **52**, 12–34 (2010).
[8] K. Kwak, S. Park, I. J. Finkelstein, and M. D. Fayer, J. Chem. Phys. **127**, 124503 (2007).
[9] K. Kwak, D. E. Rosenfeld, and M. D. Fayer, J. Chem. Phys. **128**, 204505 (2008).
[10] S.-H. Shim and M. Zanni, Phys. Chem. Chem. Phys. **11**, 748–761 (2009).
[11] P. Hamm and M. T. Zanni, *Concepts and Methods of 2D Infrared Spectroscopy* (Cambridge University Press, Cambridge; New York, 2011).

[12]M. Khalil, N. Demirdoven, and A. Tokmakoff, Phys. Rev. Lett. **90**, 047401 (2003).
[13]J. B. Asbury, T. Steinel, C. Stromberg, K. J. Gaffney, I. R. Piletic, A. Goun, and M. D. Fayer, Chem. Phys. Lett. **374**, 362–371 (2003).
[14]V. Volkov, R. Schanz, and P. Hamm, Opt. Lett. **30**, 2010–2012 (2005).
[15]A. D. Bristow, D. Karaiskaj, X. Dai, T. Zhang, C. Carlsson, K. R. Hagen, R. Jimenez, and S. T. Cundiff, Rev. Sci. Instrum. **80**, 073108 (2009).
[16]F. Ding, P. Mukherjee, and M. T. Zanni, Opt. Lett. **31**(19), 2918–2920 (2006).
[17]S. M. Gallagher Faeder and D. M. Jonas, J. Phys. Chem. A **103**, 10489–10505 (1999).
[18]L. P. DeFlores, R. A. Nicodemus, and A. Tokmakoff, Opt. Lett. **32**, 2966–2968 (2007).
[19]S. Yan and H. S. Tan, Chem. Phys. **360**, 110–115 (2009).
[20]J. A. Myers, K. L. Lewis, P. F. Tekavec, and J. P. Ogilvie, Opt. Express **16**(22), 17420–17428 (2008).
[21]J. Rehault, V. Zanirato, M. Olivucci, and J. Helbing, J. Chem. Phys. **134**, 124516 (2011).
[22]W. Xiong and M. T. Zanni, Opt. Lett. **33**, 1371–1373 (2008).
[23]A. Weiner, Rev. Sci. Instrum. **71**, 1929 (2000).
[24]C. Hillegas, J. Tull, D. Goswami, D. Strickland, and W. Warren, Opt. Lett. **19**, 737–746 (1994).
[25]M. Fetterman, D. Goswami, D. Keusters, W. Yang, J. K. Rhee, and W. Warren, Opt. Express **3**, 366–375 (1998).
[26]P. Tian, D. Keusters, Y. Suzaki, and W. S. Warren, Science **300**, 1553–1555 (2003).
[27]S. H. Shim, D. B. Strasfeld, E. C. Fulmer, and M. T. Zanni, Opt. Lett. **31**, 838–840 (2006).
[28]S. H. Shim, D. B. Strasfeld, and M. T. Zanni, Opt. Express **14**, 13120–13130 (2006).
[29]H.-S. Tan, J. Chem. Phys. **129**, 124501 (2008).
[30]C. T. Middleton, P. Marek, P. Cao, C.-c. Chiu, S. Singh, A. M. Woys, J. J. de Pablo, D. P. Raleigh, and M. T. Zanni, Nat. Chem. **4**, 355–360 (2012).
[31]P. Hamm, R. A. Kaindl, and J. Stenger, Opt. Lett. **25**, 1798–1800 (2000).
[32]D. Keusters, H.-S. Tan, and W. S. Warren, J. Phys. Chem. A **103**, 10369–10380 (1999).
[33]C. E. Shannon, Proc. IEEE **86**, 447–457 (1998).
[34]Z. Zhang, K. L. Wells, E. W. J. Hyland, and H.-S. Tan, private communication (2012).
[35]I. E. Pomestchenko, D. E. Polyansky, and F. N. Castellano, Inorg. Chem. **44**, 3412–3421 (2005).
[36]H. Akaike, IEEE Trans. Autom. Control **19**, 716–723 (1974).
[37]S. Park, K. Kwak, and M. D. Fayer, Laser Phys. Lett. **4**, 704–718 (2007).
[38]A. L. Sturlaugson, K. S. Fruchey, and M. D. Fayer, J. Phys. Chem. B **116**, 1777–1787 (2012).
[39]A. L. Sturlaugson, K. S. Fruchey, S. R. Lynch, S. R. Aragon, and M. D. Fayer, J. Phys. Chem. B **114**, 5350–5358 (2010).
[40]K. W. Kwak, S. Park, and M. D. Fayer, Proc. Nat. Acad. Sci. U.S.A. **104**, 14221–14226 (2007).
[41]K. S. Schweizer and D. Chandler, J. Chem. Phys. **76**, 2296–2314 (1982).
[42]E. M. Grumstrup, S. H. Shim, M. A. Montgomery, N. H. Damrauer, and M. T. Zanni, Opt. Express **15**, 16681–16689 (2007).